Earth and Space Science

RESEARCH ARTICLE
10.1029/2022EA002612

Validation of OSCAR Surface Currents in the Western Arctic Marginal Seas Against Saildrone Observations

Nan-Hsun Chi[1], Dongxiao Zhang[1,2], and Chidong Zhang[1]

[1]NOAA Pacific Marine Environmental Laboratory, Seattle, WA, USA, [2]The Cooperative Institute for Climate, Ocean and Ecosystem Studies, University of Washington, Seattle, WA, USA

Key Points:

- This study validates Ocean Surface Current Analysis Real-time (OSCAR) satellite derived surface currents in the western Arctic, including the very shallow waters, by saildrones
- High vector correlation but larger vector difference between OSCAR and saildrone currents often occur in strong topography guided currents
- Low vector correlation occurs at weaker currents, over the shallow Hanna Shoal, and near fresher waters due to ice melt and river discharge

Correspondence to:
N.-H. Chi,
nan-hsun.chi@noaa.gov

Citation:
Chi, N.-H., Zhang, D., & Zhang, C. (2023). Validation of OSCAR surface currents in the western Arctic marginal seas against saildrone observations. *Earth and Space Science*, *10*, e2022EA002612. https://doi.org/10.1029/2022EA002612

Received 29 SEP 2022
Accepted 24 JUL 2023

Author Contributions:
Conceptualization: Nan-Hsun Chi
Data curation: Nan-Hsun Chi
Formal analysis: Nan-Hsun Chi
Funding acquisition: Chidong Zhang
Methodology: Nan-Hsun Chi, Dongxiao Zhang, Chidong Zhang
Software: Nan-Hsun Chi
Supervision: Dongxiao Zhang, Chidong Zhang
Validation: Nan-Hsun Chi
Visualization: Nan-Hsun Chi
Writing – original draft: Nan-Hsun Chi
Writing – review & editing: Nan-Hsun Chi, Dongxiao Zhang, Chidong Zhang

Abstract The western Arctic marginal seas undergo large seasonal variation, but are very challenging to observe directly due to sea ice and shallow depths. Deployments of several saildrone uncrewed surface vehicles in the summers of 2018 and 2019 provided unique opportunities to validate the satellite-derived near surface currents, Ocean Surface Current Analysis Real-time (OSCAR), in the western Arctic marginal seas against in situ upper ocean current measurements. Overall, OSCAR current is biased low (by 5.3 cm/s) with significant noise. Higher vector correlation estimated by the cosine similarity and speed differences often occur where stronger currents (often topography-steered) are observed. Such differences reveal that the data set resolvability depends on spatial and temporal resolutions, smoothing, and latitudes, suggesting that OSCAR is able to depict the major current systems but significantly underestimates their strength. Poorer vector correlation occurs at weaker current regimes (<10 cm/s), over the shallow Hanna Shoal, near fresher water due to ice melt and river discharge. The latter two water class regimes highlight the importance of salinity contribution to the buoyancy force which is neglected in the OSCAR formulation.

Plain Language Summary It is challenging to make direct measurements in the western Arctic marginal seas, which undergo large seasonal swings, because of the sea ice and shallow depths. We validate the satellite-derived surface current product, Ocean Surface Current Analysis Real-time (OSCAR), against observations from saildrone uncrewed surface vehicles in the western Arctic marginal seas cruising in summers of 2018 and 2019. Overall, OSCAR current is biased low and noisy. Higher current direction relation and speed differences often occur where stronger currents are observed. Such differences suggest that the reliability of OSCAR depends on several factors. It also suggests that OSCAR is able to depict the major current systems but significantly underestimates their strength. Poorer current direction relation occurs at weaker current regimes, over the shallow Hanna Shoal, near fresher water due to ice melt and river discharge. The latter two regimes highlight the importance of salinity information, which however, is neglected in the OSCAR model.

1. Introduction

The near surface currents in the western Arctic marginal seas (i.e., the Bering, Chukchi, and Beaufort Seas) play important roles in various geophysical phenomena, such as the transport of heat, salt (e.g., Woodgate, 2018; Woodgate & Peralta-Ferriz, 2021), and sea ice (DeRepentigny et al., 2020; Krumpen et al., 2019). Monitoring the surface current variation is therefore essential for studying the fate of the Pacific-origin waters into the Arctic basin and its impact on the Arctic ecosystem (Stabeno, 2019).

Accurate knowledge of the upper surface currents systems in the western Arctic marginal seas is important in estimating the transport and fluxes of various physical properties and matters. The state-of-art global near surface ocean currents products (i.e., Ocean Surface Current Analysis Real-time (OSCAR)) are not directly measured by satellites but derived from the satellite measurements using simplified formulation (Bonjean & Lagerloef, 2002). As the sea surface height measurements in the high latitudes become available after 2010s from emergence of new satellite products and now being used (i.e., Cryosat-2) in the latest OSCAR near surface current products, these large-scale near surface current estimates are extended to polar oceans. On the other hand, satellite observations show declining Arctic sea ice extent for all months (Serreze & Stroeve, 2015; Stabeno & Bell, 2019), exposing more ice free open ocean areas. The shortened ice season (Wang et al., 2018) are related to the greater rising of surface temperatures in the Arctic than the global mean surface temperature (Richter-Menge et al., 2019; Serreze & Francis, 2006). Climate forecast models suggest that in the Arctic the surface air temperature will continue to rise at a much faster rate and the summertime sea-ice extent will continue to decline (Alexander

et al., 2018; Jeffries et al., 2013). The spatial extent and the length of direct air-sea interaction in the ice-free Arctic are increasing, and may eventually become normal during summer in a warmer climate. For advancing the understanding of geophysical phenomena in the increasingly ice-free Arctic, including the western Arctic marginal seas, validating satellite-derived near surface products at high latitudes against in situ measurements is important. The western Arctic marginal seas feature many shallow shelf regions and mobile sea ice, which not only prevent Argo float measurements but also limit research ships from complete surveys. Therefore, in situ observations are very challenging. Saildrone uncrewed surface vehicles (USVs) provide a unique opportunity to measure air-sea interaction over the very shallow waters on the shelf and ice edge in western Arctic marginal seas. Saildrones are wind and solar powered vehicles that allow deployments lasting up to 12 months and provide high quality, near real-time, multivariate upper ocean and atmospheric observations (Zhang et al., 2019). The primary goal of this work is using the USVs deployments to validate the satellite-derived ocean surface current products, OSCAR, in the western Arctic marginal seas. Our analysis should be taken as a preliminary step in the comparison of large scale gridded upper ocean current data to encourage future research and application in this region.

In this study we focus on subsurface current velocities measured by current profilers described in Section 2.1. These saildrone provide valuable and rare in situ current observation in the seasonal ice zone or gaps of ship observations. These observations are instrumental in advancing our knowledge for further development and verification of satellite observation, satellite-derived data products, and numerical models. Recent studies used two saildrones to validate various satellite SST products and SMAP SSS products in the western Arctic (Vazquez- Cuervo et al., 2021, 2022). As the satellite-based products evolve constantly with emergence of new satellites and frequent changes of algorithms for improving their absolute accuracy, it is vital to do periodic validation against in situ data. Among eight of L4 satellite SST products, NOAA/NCEI DOISST and the RSS MWOI SST are shown to have better relative accuracy against saildrone. Also, the SMAP SSS products are shown to resolve the runoff signal associated with the Yukon River discharge with high correlation between SMAP products and saildrone 0.5 m salinity. Both MWOI SST and SMAP SSS products from Remote Sensing System (RSS) described in 2.3 are therefore chosen to be used in this study.

The manuscript is organized as follows. Section 2 describes the data and methods. Section 3 presents the results. Section 4 summarizes this paper.

2. Data and Methods

2.1. In Situ Saildrone Data

In situ data used in this study are from two saildrones deployed in July–September of 2018 (1020, 1021) and three saildrones (1035, 1036, 1037) deployed in May - September 2019 (Chiodi et al., 2021). They were launched from Dutch Harbor, Alaska crossed the Bering Strait into the Chukchi Sea (and Beaufort Sea in 2019) and headed south for recovery as the sunlight hours became short (Figures 1 and 2).

The surface current is measured by the downward looking 300 kHz Workhorse WHM300-I-UG1 acoustic Doppler current profilers (ADCP) mounted on the keels of the five saildrones. The vertical resolution of the ADCP data are 2 m. The 5-min averaged ADCP currents are analyzed here. To save power, the ADCP on 1036 and 1037 were operating at 50% duty cycle, with the ADCP turned on and off for 5 min every 10 min.

The saildrone ADCP data is often easier to process than those of the ship-board ADCP. The saildrone's transiting speed is slow—on average speed of 0.96 m/s, or ∼18% of the average wind speed at 5.4 m/s during the 2019 deployment (Chiodi et al., 2021). This quiet vehicle is less affected by bubble issues (Joseph, 2014). The ADCP data are generally reliable ∼6 m below the sea surface, determined by the depth of the transducer (1.8 m) and the blanking distance (4.2 m) of the ADCP. Depending on the echo intensity, ADCP data typically extend to 60–100 m depth, ideal for survey of the entire water column on the shelf. The saildrone ADCP has onboard motion correction for preliminary quality control before the data are sent to the data center in near real time. The motion correction based on the GPS aided Inertial Measurement Unit (IMU) measurements is validated, and fine-tuned if needed based on the bottom tracking of the ADCP performed at the deployment and recovery of the saildrones (Zhang et al., 2023). However, additional steps, including removing data below the ocean floor, or where echo intensity is too small, or where the vertical velocity is too large, are necessary to remove unrealistic current estimates and to achieve an accuracy of 2–3 cm/s or better.

The near surface temperature and salinity were measured at a nominal depth of 0.5 m by two saildrones in summer 2018 and three saildrones in summer 2019. The unpumped RBR sensors were available in both years

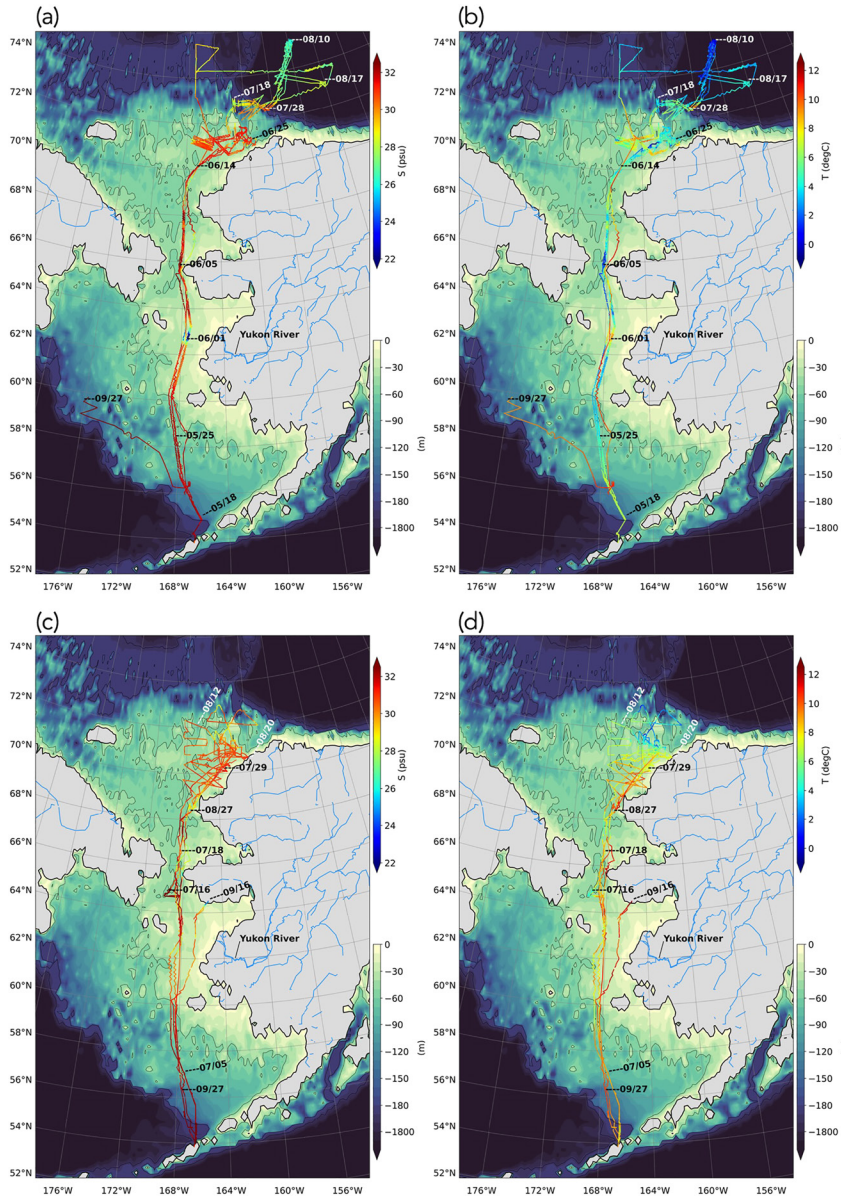

Figure 1. Three saildrone tracks (1035, 1036, 1037) in 2019 colored by (a) saildrone 0.5 m temperature and (b) saildrone 0.5 m salinity. Two saildrones (1020, 1021) in 2018 colored by (c) saildrone 0.5 temperature and (d) saildrone 0.5 m salinity. The contour background is the bathymetry. The thin black contours are depth contours of −50, −200, and −1,000 m. The magenta labels are the dates (mm/dd) of the locations of 1036 in 2019 and of 1020 in 2018.

and the pumped SBE sensors were available in 2019. Here we use RBR measurements in 2018 and SBE measurements in 2019. The RBR data are available every 10 min on 1020, 1021 and the SBE data are available every 5 min on 1035, 1036, 1037.

The temperature and salinity data analyzed are 1-min averages of 1-Hz measurements. Simple QC are applied to the temperature and salinity data by removing those with large 1-min standard deviation (0.1°C for temperature and 0.05 psu for salinity).

2.2. OSCAR Data

Ocean Surface Current Analysis Real-time (OSCAR) is a global near-surface (nominal 150 depth at 15 m) ocean current product derived from sea surface height, ocean surface vector winds and sea surface temperature observed

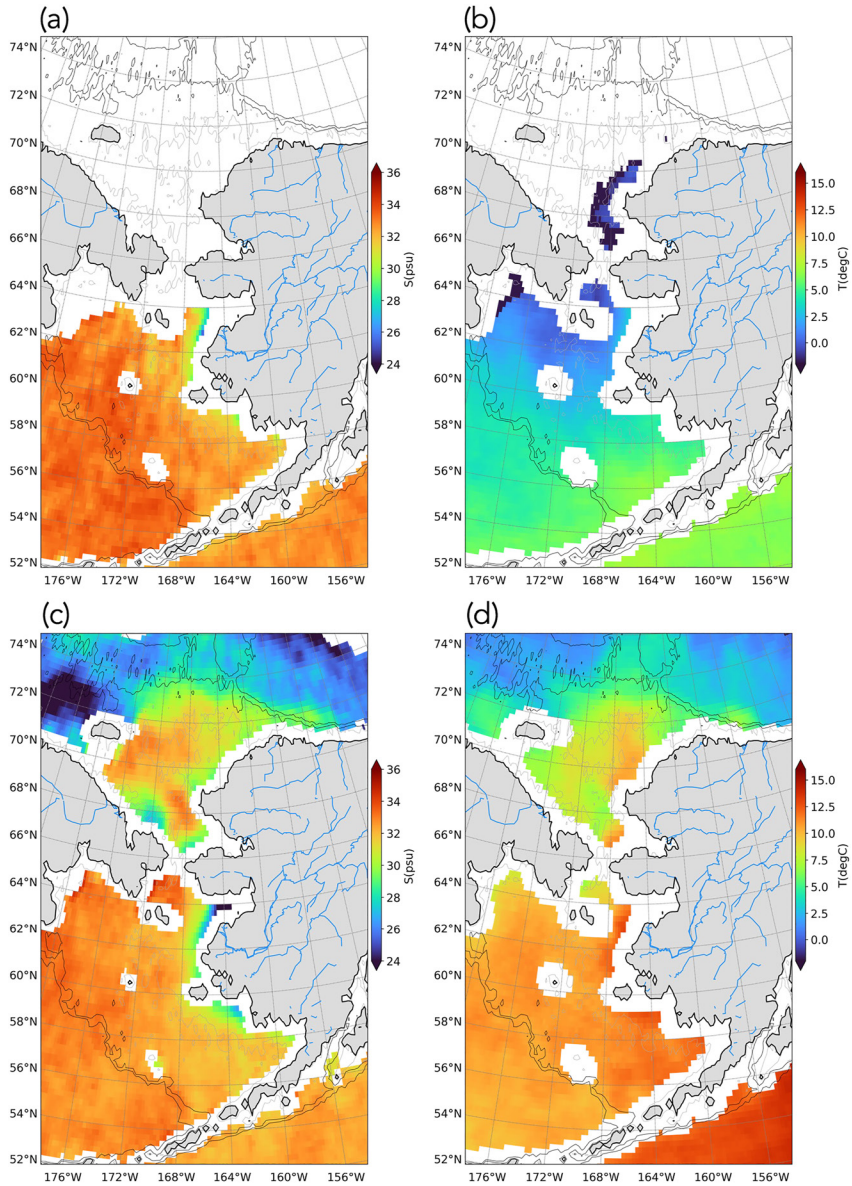

Figure 2. Satellite maps of (a, c) sea surface salinity and (b, d) sea surface temperature on (a, b) 2019/05/15, and (c, d) 2019/09/15. The bathymetry contour levels are the same as in Figure 1.

by various satellites and in situ instruments (ESR: Dohan, Kathleen, 2021). The model formulation combines geostrophic, Ekman and thermal wind dynamics (e.g., the local acceleration and non-linearities are not represented. Bonjean & Lagerloef, 2002). Its version 2.0, on ¼ degree with a 1-day resolution, is used in this study.

The OSCAR calibration and validation (https://www.esr.org/research/oscar/validation/) using both 15 m drogued drifters and moorings suggest that its known problem areas fall in 3 main categories: eddy-dead regions such as the Alaskan Gyre, the meridional component around the equator and near coasts. Smoothing in creation of the regular gridded source data and during the calculation of spatial gradients would consistently underestimate the speeds compared to those of drifters, generally by 50%–60% globally. Parts of the western Arctic marginal seas could fall in the last case where the model is not accurate very close to coastlines or ice, since source satellite signals can be corrupted there.

2.3. Satellite Sea Surface Temperature and Salinity Data

Sea surface temperature (SST) and sea surface salinity (SSS) data are both from Remote Sensing Systems (RSS) (Meissner et al., 2022). The SST product is the RSS Microwave (MW) OI SST version 5.1 (daily mean). The SSS data is SMAP version 5.0 Level 3 8-day running mean by RSS on 1-day nominal resolution. Both SST and SSS products are distributed in a 0.25° rectangular projection. This latest SMAP RSS version uses a new sea ice flag and sea ice correction including detection of large drifting icebergs.

2.4. Satellite Ancillary Data—AVISO FES 2014 Tide Database

AVISO FES 2014 tides database is used to remove the barotropic tidal current from the in situ saildrone measured current. FES2014 was produced by Noveltis, Legos and CLS and distributed by Aviso+, with support from Cnes (https://www.aviso.altimetry.fr/). It is a global tide solution that uses finite element mesh, T-UGO barotropic model and data assimilation of altimetry and tidal gauges.

Removing tidal currents are necessary in order to compare with OSCAR, the non-tidal near surface currents products. Previous studies have documented the regional-dependent characteristics of tides along the western Arctic marginal seas (i.e., Foreman et al., 2006; Huang et al., 2011; Mofjeld, 1986). The northeastern Chukchi Sea appears to be non-tidal and is often dominated by currents driven by synoptic weather patterns. Tidal currents are also weak in the eastern Chukchi shelf (amplitude <5 cm/s). In the Bering Sea tidal current amplitudes are significant (about 40 cm/s) especially near coastlines of the Bristol Bay, Kuskokwim Bay and Norton Sound.

2.5. Collocation and Statistical Evaluation of OSCAR

We use nearest-neighbor interpolation to first match each saildrone measurements (5- or 10-min) with the OSCAR gridded data in time and space. For each unique gridded OSCAR data point, all saildrone data are averaged within that grid cell for a single match-up saildrone data point. The geophysical variability arising from temporal, spatial, and definitional mismatch between satellite-derived surface current and reference data, that is, saildrone surface current data, are expected but not quantified. Therefore, the differences arising from the mismatches between the ¼ degree, daily OSCAR and the collocated and usually few-hour averaged saildrone surface current may not be trivial compared to the systematic uncertainty between the two datasets when sub-footprint features are present for example, fronts, eddies. Figure 3 shows the time series of the collocated saildrone 10–20 m layer averaged current vectors in 2019 around the OSCAR grids and their vector differences. The evaluation of the differences between OSCAR and saildrone current speed are quantified objectively by several statistical metrics including bias, root-mean-square error (RMSE), standard deviation of the errors (SDE), and signal-to-noise ratio (SNR) in Table 1. The definitions of the statistical metrics follow Vazquez-Cuervo et al. (2022). The fractional differences of current speed are also estimated by ratio of the speed difference between the collocated OSCAR and saildrone to the reference value by saildrones. The vector correlation is the cosine similarity as the cosine of the angle between the collocated OSCAR and saildrone current vectors.

3. Results

Figures 1a and 1b shows three saildrone tracks during summer 2019. They were deployed from Dutch Harbor in mid-May and made their way off Alaska's west and northwestern coastline through the Bering Sea and up through the Bering Strait around 5 June 2019. Then the saildrone 200 stayed in the Chukchi Sea shelf until July 2019 and reached the farthest northern latitude ~75.5 N in the Beaufort Sea in August before returning to Dutch Harbor in early October. The near surface waters are remarkably colder and fresher in the Beaufort Sea than those on the Bering and Chukchi shelves (Figures 1a, 1b and 2). The saildrones also measured the very warm and fresh surface waters, associated with seasonal warming and freshening, west of Yukon-Kuskokwim delta (Y-K delta) in early June 2019 (Vazquez-Cuervo et al., 2021, 2022). The surface waters on the shelf are significantly warmed in 3 months of the saildrone deployment (Figures 1 and 2); the Bering Sea shelf is freshened especially near the Alaskan coast.

The saildrones in summer 2018 went similar routes in the Bering Sea and Chukchi Sea from July to the end of September but did not reach the Beaufort Sea. The fresh and warm signals associated with Yukon River discharge are not as obvious as in July 2019. The difference is consistent with the climatology of the seasonal variation

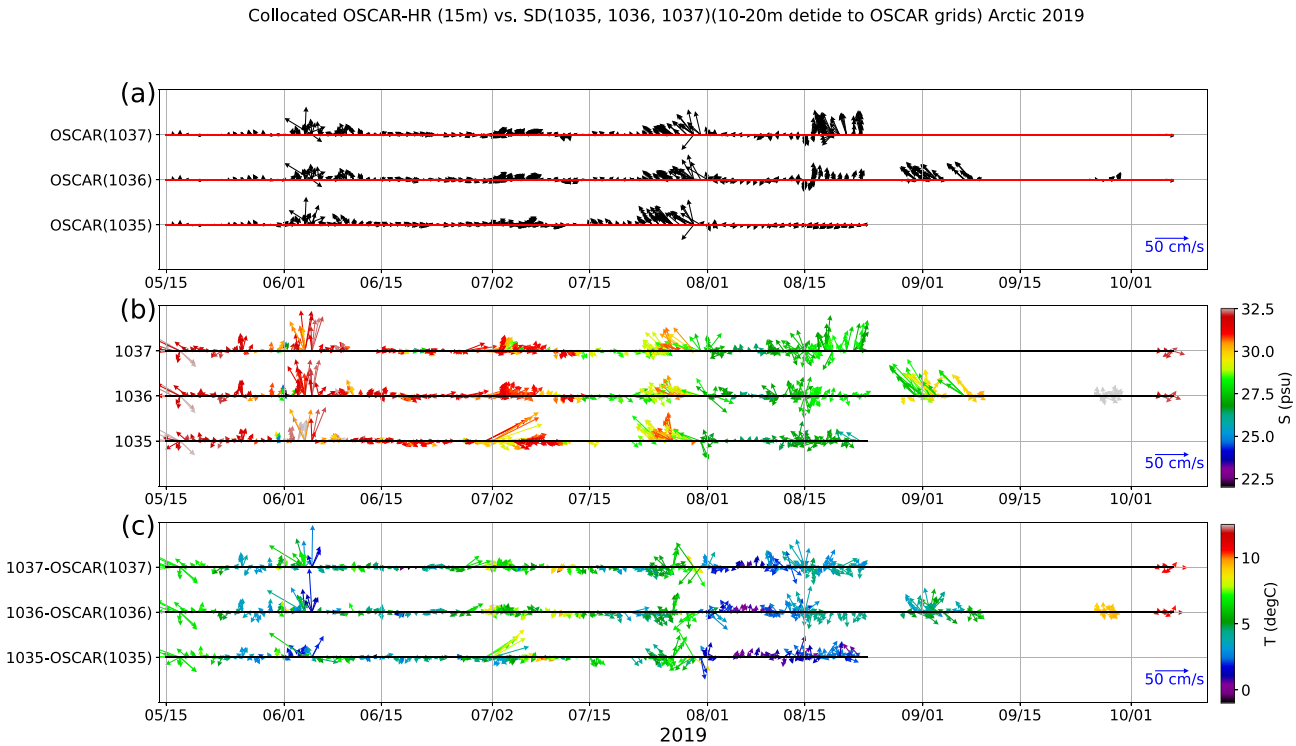

Figure 3. The time series of current vectors of (a) OSCAR 15 m current in time and space along the saildrone track, (b) saildrones 10–20 m current vectors averaged around each OSCAR ¼ degree data grid within 1 day to match OSCAR grids colored with saildrone 0.5 m salinity, and (c) their vector differences (saildrone–OSCAR) colored with saildrone 0.5 m temperature. OSCAR(1035), OSCAR(1036), and OSCAR(1037) are the corresponding OSCAR current in time and space along the saildrone track.

west of the Y-K delta (Figure 9 of Vazquez-Cuervo et al., 2022), with SSS dipping seasonally around mid-May to mid-June and increasing afterward, and SST increasing seasonally from April to July.

3.1. Overall Comparison Between Saildrone and OSCAR Data Sets

Figure 4 summarizes the overall data distribution in direction bins of every 22.5° and several specific subsets of the collocated saildrone 10–20 m layer averaged and OSCAR 15 m current data, the current speed difference and vector correlation between the two current datasets. The spokes represent the direction of which current vectors are toward. Colors along the spokes indicate the parameters specified (i.e., speed, speed difference, or vector correlation). The length of each spoke and its colored segment represents the percentage occurrence of the currents (as numbered) flowing toward a particular direction at a given parameter range. Their overall speed difference is notable (Figures 4a–4c), with OSCAR currents weaker than saildrones by 5.3 cm/s (Table 1). Underestimation can result from smoothing and spatial resolution of satellite data in creating the regular-grid OSCAR products, and the coarse spatial resolution of the wind input. 67% of the collocated velocity pairs are correlated (with direction difference within 67.5°), and is consistent between using 2018 current data only (67%) and 2019 only (70%). The slope of the linear regression line indicates that OSCAR in general underestimates the current speeds and their zonal or meridional velocities by 50%–100% (Figure 5). The negative mean (−0.08) and median (−0.34), and the right-skewed of the fractional difference against saildrone current speed indicates OSCAR's overall underestimation relative to the saildrones (Figure 5d). The saildrone current speed distribution is also more dispersed than the OSCAR current speed (Figure 5e). The RMSD, which characterizes the variability in the difference of the two datasets, is 11 cm/s. The SDE, in which the mean bias (5.3 cm/s) was removed, is 9.6 cm/s. RMSD and SDE are both more profound than the mean bias, and on the same order of magnitude as the observed SD, suggesting notable speed difference from observation. Part of the systematic differences could be attributed to the geophysical variability arising from temporal, spatial mismatch between the satellite and saildrone data when the mesoscale or submesoscale features are present; however, they are not quantified here. The signal-to-noise ratio (SNR), which is inversely proportional to SDE, is 0.8. In fact, the SNR of all subsets

Table 1
Summary of Statistical Differences Between the Collocated OSCAR and Saildrone Current Speed and Vector Correlation Under Several Specific Subsets Described in the Leftmost Column With the Number of Pairs in the Parenthesis

	Obs. SD (cm/s)	Bias (cm/s)	RMSD (cm/s)	SDE (cm/s)	SNR (cm/s)	Percentage of current vector correlation (%)		
						$R > 0.38$	$\|R\| \leq <0.38$	$R < -0.38$
Overall (2267)	11.5 (11.0–12.2)	−5.3 (−5.4–−5.1)	11.0 (10.7–11.1)	9.6 (9.4–9.7)	0.80 (0.77–0.81)	68.8 (68.1–69.6)	13.9 (13.4–14.4)	17.3 (16.7–17.9)
Current >30 cm/s (237)	10.3(9.0–12.4)	−20.6 (−21.2–19.9)	24.2 (23.5–24.9)	12.8 (12.2–13.2)	0.80 (0.77–0.84)	87.8 (86.0–89.5)	5.1 (4.0–6.0)	7.2 (6.0–8.5)
Current <10 cm/s (896)	2.4 (2.3–2.5)	0.8 (0.67–0.85)	4.8 (4.7–4.9)	4.8 (4.7–4.9)	0.92 (0.90–0.93)	56.1 (55.1–57.1)	19.2 (18.4–19.9)	24.7 (23.8–25.5)
Cold fresh $T < 2C$, $S < 27$ psμ (127 from 2019)	7.1 (6.1–8.2)	−3.2 (−3.6–−2.9)	8.0 (7.4–8.4)	7.3 (6.8–7.6)	0.38 (0.35–0.40)	43.3 (39.9–45.3)	24.4 (21.6–27.0)	32.3 (30.3–35.7)
Yukon River Discharge $T > 5C$, $S < 28$ psμ (12 from 2019)	4.2 (3.1–5.5)	−4.8 (−5.7–−4.3)	7.2 (6.6–7.8)	5.4 (4.8–5.8)	0.40 (0.35–0.46)	58.3 (50.0–67.8)	33.3 (30.0–40.0)	8.3 (0.0–10.0)
Hanna Shoal >−30 m (44)	4.9 (4.1–5.9)	−4.8 (−5.2–−4.3)	7.1 (6.7–7.3)	5.3 (4.8–5.4)	0.60 (0.57–0.64)	54.5 (50.0–60.0)	13.6 (10.0–15.0)	31.8 (25.0–35.0)
>−30 m (96)	8.7 (7.4–10.7)	−6.0 (−6.5–−5.5)	10.9 (10.2–11.3)	9.0 (8.4–9.4)	0.46 (0.42–0.50)	58.3 (55.3–62.4)	11.5 (9.4–12.9)	30.2 (26.0–32.9)

Note. Obs. SD is the observed current speed by saildrones. RMSD is root-mean-square-difference. Bias is the mean residual difference, OSCAR-SD. SDE is the standard deviation of errors in which the mean bias error is removed. SNR is the signal-to-noise ratio. R is the vector correlation coefficient described in Figure 4. $R > 0.38$, $|R| \leq 0.38$, and $R < -0.38$ refers to the angle between collocated vectors smaller than 67.5°, between 67.5° and 112.5°, and between 112.5° and 180° respectively. The 95%-confidence intervals are shown in the parenthesis for each calculated metric quantity through a bootstrap method.

is smaller than 1, indicating that the noise of OSCAR current speed overwhelms the real signals.

3.2. Comparisons Between Saildrone and OSCAR DataSets in Different Current Speed Regimes

The strong current regime (current speed >30 cm/s) is observed mostly in bathymetry guided flows, that is, in the Bering Strait where currents flow northward in early June 2019, upstream Barrow Canyon where currents flow eastward in July 2019, and on the Chukchi Slope where Chukchi Slope Currents flow northwestward in the end of July 2019 (Figures 1 and 3). Their vector correlation is well above average (64% of vector correlation is >0.92, i.e., less than 22.5- degree deviation from each other). The negative bias and RMSD of the OSCAR current speed are of the same order of magnitude (O(20 cm/s)) and significantly larger than average (Figures 4e–4g, Table 1). This phenomenon is consistent with the lower-than-1 linear regression slope and small intercept (Figure 5a). The SDE is half of the RMSE and larger than the observed SD, indicating the differences in current speed of the strong current regime is significant and considerably contributed by underestimation.

For the weak current regime (current speed <10 cm/s), the overall vector correlation is lower than average, more than 40% is either orthogonal or negatively correlated. In contrast, OSCAR current speed is positively biased by 0.8 cm/s, also indicated by the positive intercept of y-axis in Figure 5a. The RMSD and SDE are twice the observed SD. It suggests that for the weaker current regime the OSCAR current speed is significantly different from observation and with slight overestimation.

3.3. Comparisons Between Saildrone and OSCAR Data Sets in Different Water Classes or Areas

The collocated OSCAR and saildrone currents show poorer vector correlation than average at the cold fresh water lenses from ice melting and warm fresh Yukon River discharge (Figures 4p and 4t, Table 1). The RMSD and SDE of current speed for both water classes are slightly larger than the observed SD, indicating significant current speed difference. The SNR is reduced to half compared to the overall statistics (0.80 for overall; 0.38 for cold fresh and 0.40 for warm fresh water classes), indicating the OSCAR current speeds in these two surface water classes are overwhelmed by noise. These lighter surface water lenses from ice melting or river outflow that increase the near surface stratification are commonly present in summertime. However, the buoyancy force is only a function of SST but not SSS in OSCAR formulation (Bonjean & Lagerloef, 2002). Since salinity dominates the density variation in the cold-water regime, it suggests that the salinity contribution to the buoyancy gradient to the thermal wind velocities could be significant. Large salinity stratification near the surface could also induce large current velocity shear near the surface, which could potentially modulate the ocean response to the winds, and their air-sea momentum transfer.

On the other hand, there are areas with very shallow bathymetry on the Chukchi Sea shelf near the west Alaskan coast where the saildrones had chances to make measurements in 2018 and 2019. The vector correlation at the shallow bathymetry on the eastern Chukchi shelf is similar to the overall statistics (Table 1). The vector correlation is poorer around Hanna Shoal where the bathymetry is also shallow and current speed is slightly weaker. The RMSD and SDE of both subsets are slightly larger than the observed SD, and with reduced SNR compared to the

10.1029/2022EA002612

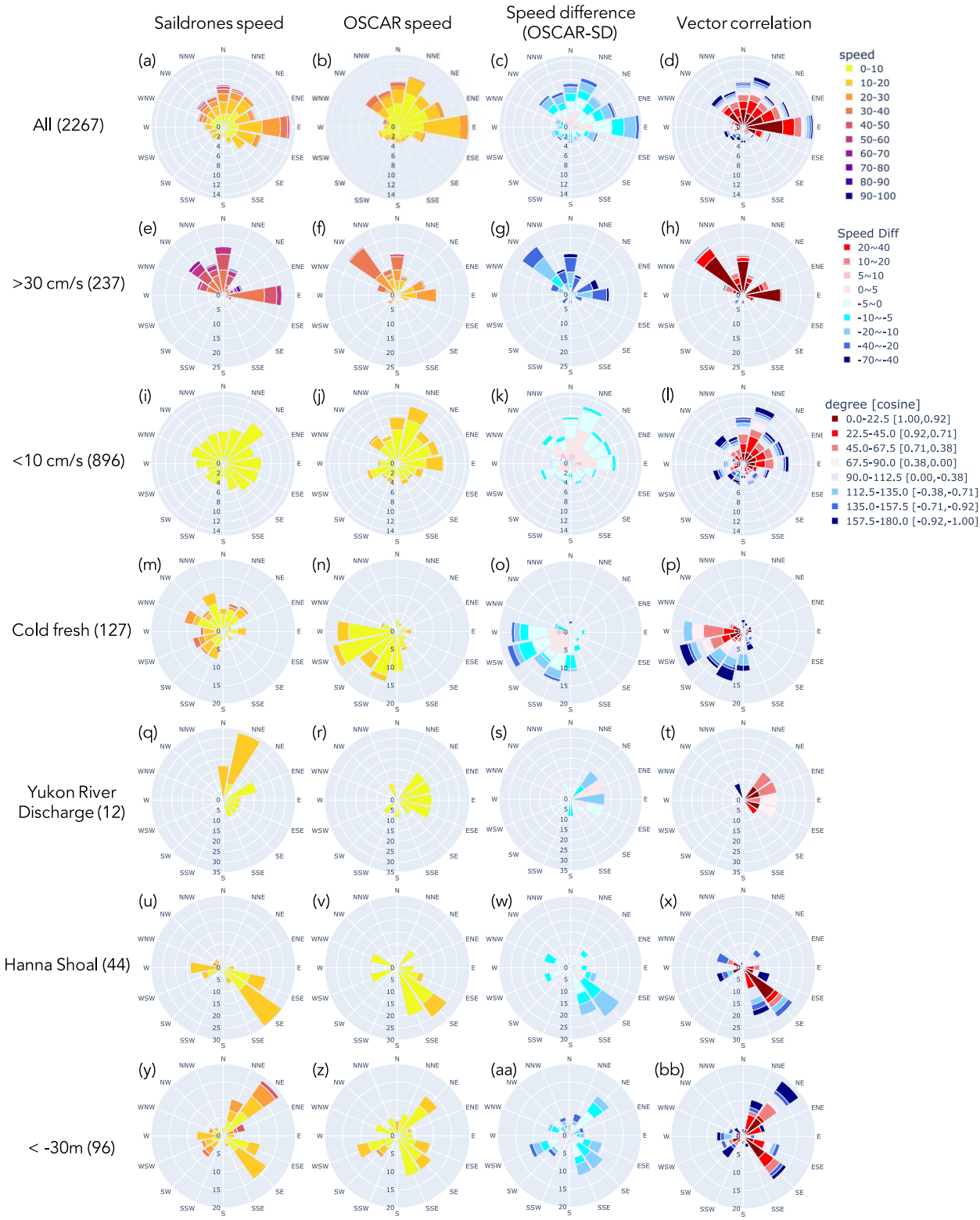

Figure 4.

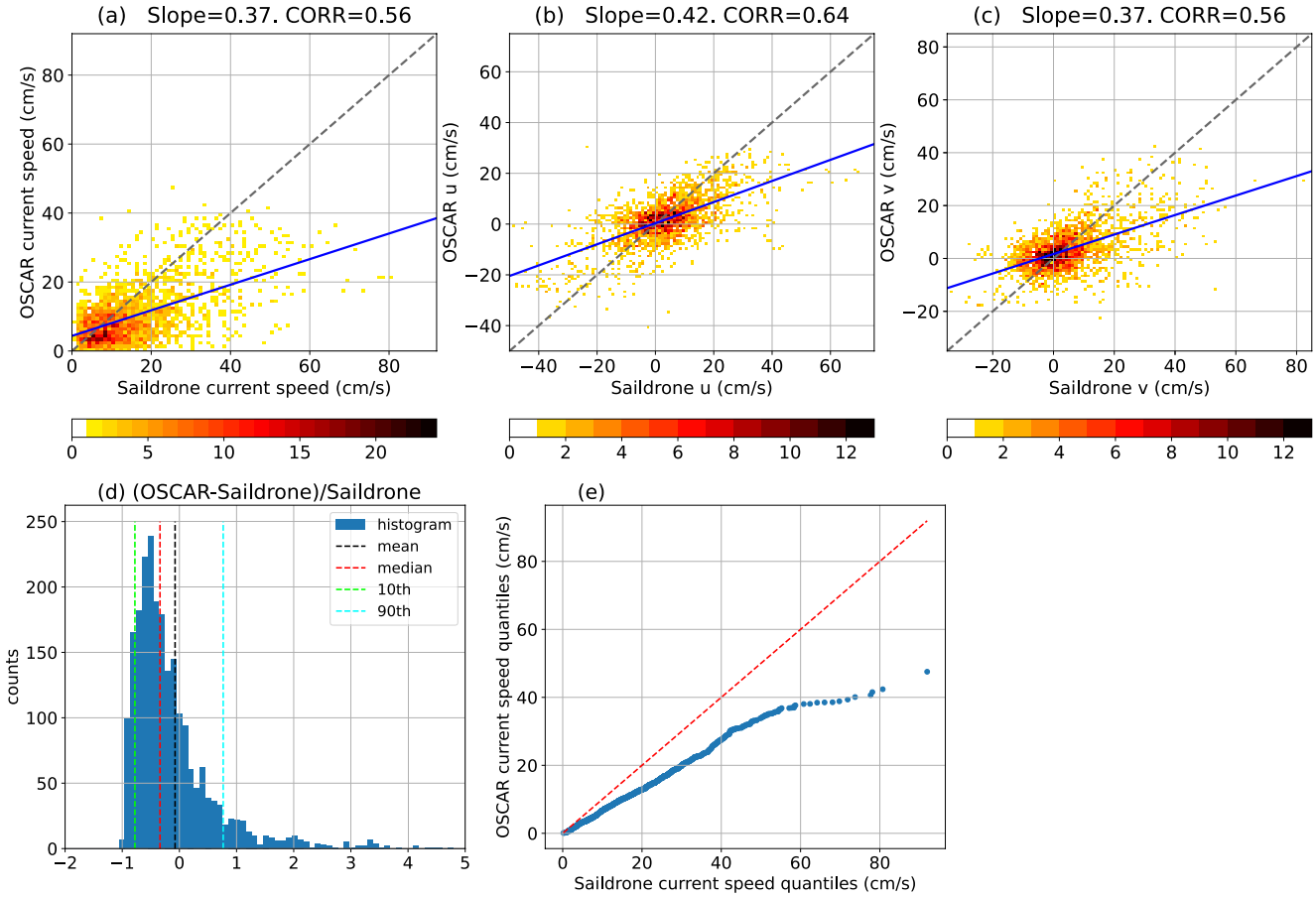

Figure 5. 2D histogram of (a) current speed (b) zonal current velocity and (c) meridional current velocity between the collocated saildrones and OSCAR data. The blue solid line is the linear regression line. The unit of the colors is the number. (d) The fractional differences against saildrone current speed and their mean (black dashed line), median (red dashed line), 10th and 90th percentiles (lime and cyan dashed lines, respectively). (e) The quantile-quantile plot comparing saildrone and OSCAR current speed probability distribution by their quantiles against each other.

overall statistics. Similar to the aforementioned two water classes, the OSCAR current speeds in the shallow water are of significant difference from observation and excessively overwhelmed by noise. Larger uncertainties near the coastlines, within 100 km, are known problems in the OSCAR model (Section 2.2).

4. Summary

This work presents rare upper ocean current measurements from saildrone USVs in the Bering Sea shelf, Chukchi Sea shelf and slope regions, and Beaufort Sea, where shallow waters can only be surveyed by some research vessels with specialized equipment or shallow draft. We use saildrone in situ data from the summers of 2018 and 2019 to validate the OSCAR satellite derived current products. This work quantifies the uncertainty of the OSCAR near surface currents and highlights the regimes to expect larger negative biases of current speed or lower vector correlation. The overall current speed difference for the collocated OSCAR and saildrones is significant (SDE larger than the observed SD), with OSCAR under-estimating the observed speed. Particularly, the OSCAR satellite derived currents data in the western Arctic is 50%–100% lower than the observations. For comparison, globally the derived currents data is 50%–60% lower than in situ data observed from 15 m drogued

Figure 4. The wind rose plot summarizing the collocated vectors for (first column: a, e, i, m, q, u, y) saildrone 10–20 m averaged current vectors, (second column: b, f, j, n, r, v, z) OSCAR 15-m current vectors, (third column: c, g, k, o, s, w, aa) current speed difference (OSCAR - saildrone), and (last column: d, h, l, p, t, x, bb) vector correlation of the collocated pairs between OSCAR and saildrones. Each row represents the results of a specific subset of collocated vectors described in the subtitles on the left with the number of pairs in the parenthesis. The convention here is direction toward; that is, the "spoke" toward "N" represents current flowing northward. The degrees in the rightmost column subplots (c, f, i, l, o, r, u) are the angle between the collocated OSCAR and saildrone current vectors. The values in the brackets for vector correlation colorbar are the limits of the cosine similarity. The unit of current speed is cm/s.

drifters and moorings from the global network of OceanSITES. Such differences reveal that the data set resolvability depends on spatial and temporal resolution, smoothing, and latitudes. In addition, the signal-to-ratio (SNR) of the OSCAR current speeds is lower than 1 in western Arctic marginal seas, indicating an overwhelming noise level in the data set.

Higher vector correlation occurs at the strong current regime where currents are guided by the bathymetry. The negative speed bias of the strong current regime is O(20 cm/s). This implies that OSCAR is able to depict the major current systems in the western Arctic marginal seas but significantly underestimates their strength. Low vector correlation is often observed for weaker currents, for example, in the Hanna Shoal area, or in stratified surface waters from either the warm fresh river discharge or the cold fresh surface melt waters. The SNR of OSCAR is also significantly reduced in the Hanna Shoal area and the aforementioned lighter surface waters. The poor statistical results for the warm fresh river discharge or the cold fresh surface melt waters compared to the overall statistics highlight the importance of the salinity information especially in cold water regimes for the vertical momentum diffusion, though neglected in the OSCAR model.

This analysis serves as a preliminary step toward comparing and validating large scale gridded upper ocean current products to encourage future research and application in the western Arctic and other parts of the world's oceans using saildrone data. Repeated saildrone missions in key areas in the western Arctic marginal seas would be beneficial in monitoring and quantification of the Pacific water inflow rates and routes. Additionally, saildrones can be used to validate and improve the satellite-derived surface current data in high latitude oceans, enabling better estimation of surface water routes and properties in other parts of high latitude regions under a warming climate. The results also suggest the feasibility of improving the satellite-derived surface current estimation by taking satellite SSS into account.

Data Availability Statement

- The saildrone current velocity data in the 2019 Arctic mission are accessed from DOI:10.5067/SDRON-NOPP0, and https://data.pmel.noaa.gov/pmel/erddap/tabledap/sd1035_adcp_arctic_2019.html. The near surface temperature and salinity data in 2019 Arctic mission are accessed from https://data.pmel.noaa.gov/pmel/erddap/tabledap/sd1035_2019.html, https://data.pmel.noaa.gov/pmel/erddap/tabledap/sd1036_2019.html, and https://data.pmel.noaa.gov/pmel/erddap/tabledap/sd1037_2019.html.
- The saildrone current velocity data in the 2018 Arctic mission are accessed from https://data.pmel.noaa.gov/pmel/erddap/tabledap/sd1020_adcp_arctic_2018.html, and https://data.pmel.noaa.gov/pmel/erddap/tabledap/sd1021_adcp_arctic_2018.html. The saildrone near surface temperature and salinity data in 2018 Arctic mission are accessed from https://data.pmel.noaa.gov/pmel/erddap/tabledap/saildrone_arctic_2018.html.
- Ocean Surface Current Analysis Real-time (OSCAR) data area accessed from https://doi.org/10.5067/OSCAR-25F20.
- Meissner, T., F. J. Microwave OI SST data are produced by Remote Sensing Systems and sponsored by National Oceanographic Partnership Program (NOPP) and the NASA Earth Science Physical Oceanography Program. Data are available at www.remss.com.
- SMAP salinity data are produced by Remote Sensing Systems and sponsored by the NASA Ocean Salinity Science Team. Data are available at www.remss.com.
- FES2014 was produced by Noveltis, Legos and CLS and distributed by Aviso+, with support from Cnes (https://www.aviso.altimetry.fr/).

Acknowledgments
We thank the two anonymous reviewers for their valuable comments and suggestions. This is PMEL Contribution No. 5406. This publication is partially funded by the PMEL grant number X8R1U20-PDM. This publication is partially funded by the Cooperative Institute for Climate, Ocean, & Ecosystem Studies (CICOES) under NOAA Cooperative Agreement NA20OAR4320271, Contribution No. 2023-1291.

References

Alexander, M. A., Scott, J. D., Friedland, K. D., Mills, K. E., Nye, J. A., Pershing, A. J., & Thomas, A. C. (2018). Projected sea surface temperatures over the 21st century: Changes in the mean, variability and extremes for large marine ecosystem regions of Northern Oceans. *Elementa: Science of the Anthropocene*, *6*, 9. https://doi.org/10.1525/elementa.191

Bonjean, F., & Lagerloef, G. S. E. (2002). Diagnostic model and analysis of the surface currents in the tropical Pacific Ocean. *Journal of Physical Oceanography*, *32*(10), 2938–2954. https://doi.org/10.1175/1520-0485(2002)032<2938:DMAAOT>2.0.CO;2

Chiodi, A. M., Zhang, C., Cokelet, E. D., Yang, Q., Mordy, C. W., Gentemann, C. L., et al. (2021). Exploring the Pacific Arctic seasonal ice zone with saildrone USVs. *Frontiers in Marine Science*, *8*, 640690. https://doi.org/10.3389/fmars.2021.640697

DeRepentigny, P., Jahn, A., Tremblay, L. B., Newton, R., & Pfirman, S. (2020). Increased transnational sea ice transport between neighboring Arctic states in the 21st century. *Earth's Future*, *8*(3), e2019EF001284. https://doi.org/10.1029/2019EF001284

ESR: Dohan, Kathleen. (2021). Ocean surface current analyses real-time (OSCAR) surface currents - Final 0.25 degree (version 2.0). ver. 2.0 [Dataset]. PO.DAAC. https://doi.org/10.5067/OSCAR-25F20

Foreman, M. G. G., Cummins, P. F., Cherniawsky, J. Y., & Stabeno, P. (2006). Tidal energy in the Bering Sea. *Journal of Marine Research*, *64*(6), 797–818. https://doi.org/10.1357/002224006779698341

Huang, L., Wolcott, D., & Yang, H. (2011). Tidal characteristics along the western and northern coasts of Alaska. In *US hydro 2011 conference*. Retrieved from https://legacy.iho.int/mtg_docs/rhc/ArHC/ArHC3/ARHC3-3.2.4_TidalCharacteristicsAK.pdf

Jeffries, M. O., Overland, J. E., & Perovich, D. K. (2013). The Arctic shifts to a new normal. *Physics Today*, *66*(10), 35–40. https://doi.org/10.1063/PT.3.2147

Joseph, A. (2014). *Chapter 11 - Vertical profiling of currents using acoustic Doppler current profilers. Measuring ocean currents* (pp. 339–379). Elsevier. https://doi.org/10.1016/B978-0-12-415990-7.00011-9

Krumpen, T., Belter, H. J., Boetius, A., Damm, E., Haas, C., Hendricks, S., et al. (2019). Arctic warming interrupts the Transpolar Drift and affects long-range transport of sea ice and ice-rafted matter. *Scientific Reports*, *9*(5459), 1–9. https://doi.org/10.1038/s41598-019-41456-y

Meissner, T., Wentz, F. J., Manaster, A., Lindsley, R., Brewer, M., & Densberger, M. (2022). Remote sensing systems SMAP ocean surface salinities [Level 3 running 8- day], version 5.0 validated release [Dataset]. Remote Sensing Systems. https://doi.org/10.5067/SMP50-3SPCS

Mofjeld, H. O. (1986). Observed tides on the northeastern Bering Sea shelf. *Journal of Geophysical Research*, *91*(C2), 2593–2606. https://doi.org/10.1029/JC091iC02p02593

Richter-Menge, J., Osborne, E., Druckenmiller, M., & Jeffries, M. O. (2019). The Arctic, in ["State of the climate in 2018"]. *Bulletin of the American Meteorological Society*, *100*(9), S141–S145. https://doi.org/10.1175/2019BAMSStateoftheClimate.1

Saildrone (2020). Saildrone Arctic NOPP-MISST field campaign products. ver. 1.0 [Dataset]. PO.DAAC. https://doi.org/10.5067/SDRON-NOPP0

Serreze, M. C., & Francis, J. A. (2006). The Arctic amplification debate. *Climatic Change*, *76*(3–4), 241–264. https://doi.org/10.1007/s10584-005-9017-y

Serreze, M. C., & Stroeve, J. (2015). Arctic sea ice trends, variability and implications for seasonal ice forecasting. *Philosophical Transactions of the Royal Society A*, *373*(2045), 20140159. https://doi.org/10.1098/rsta.2014.0159

Stabeno, P. J. (2019). The eastern Bering Sea: Declining ice, warming seas, and a changing ecosystem [in "State of the climate in 2018"]. *Bulletin of the American Meteorological Society*, *100*, S148–S149. https://doi.org/10.1175/2019BAMSStateoftheClimate.1

Stabeno, P. J., & Bell, S. W. (2019). Extreme conditions in the Bering Sea (2017-2018): Record breaking low sea-ice extent. *Geophysical Research Letters*, *46*(15), 8952–8959. https://doi.org/10.1029/2019GL083816

Vazquez-Cuervo, J., Castro, S. L., Steele, M., Gentemann, C., Gomez-Valdes, J., & Tang, W. (2022). Comparison of GHRSST SST analysis in the Arctic Ocean and Alaskan coastal waters using saildrones. *Remote Sensing*, *14*(3), 692. https://doi.org/10.3390/rs14030692

Vazquez-Cuervo, J., Gentemann, C., Tang, W., Carroll, D., Zhang, H., Menemenlis, D., et al. (2021). Using saildrones to validate Arctic sea-surface salinity from the SMAP satellite and from ocean models. *Remote Sensing*, *13*(5), 831. https://doi.org/10.3390/rs13050831

Wang, M., Yang, Q., Overland, J. E., & Stabeno, P. (2018). Sea-ice cover timing in the Pacific Arctic: The present and projections to mid-century by selected CMIP5 models. *Deep Sea Research Part II: Topical Studies in Oceanography*, *152*, 22–34. https://doi.org/10.1016/j.dsr2.2017.11.017

Woodgate, R. A. (2018). Increases in the Pacific inflow to the Arctic from 1990 to 2015, and insights into seasonal trends and driving mechanisms from year-round Bering Strait mooring data. *Progress in Oceanography*, *160*, 124–154. https://doi.org/10.1016/j.pocean.2017.12.007

Woodgate, R. A., & Peralta-Ferriz, C. (2021). Warming and freshening of the Pacific inflow to the Arctic from 1990-2019 implying dramatic shoaling in Pacific Winter Water ventilation of the Arctic water column. *Geophysical Research Letters*, *48*, e2021GL092528. https://doi.org/10.1029/2021GL092528

Zhang, D., Chiodi, A., Zhang, C., Foltz, G. R., Cronin, M. F., Mordy, C. W., et al. (2023). Observing extreme ocean and weather events using innovative Saildrone Uncrewed Surface Vehicles. *Oceanography*. https://doi.org/10.5670/oceanog.2023.214

Zhang, D., Cronin, M. F., Meinig, C., Farrar, J. T., Jenkins, R., Peacock, D., et al. (2019). Comparing air-sea flux measurements from a new unmanned surface vehicle and proven platforms during the SPURS-2 field campaign. *Oceanography*, *32*(2), 122–133. https://doi.org/10.5670/oceanog.2019.220